

# Entropy Change through Rayleigh-Bénard Convective Transition with Rigid Boundaries

Takafumi Kita

Department of Physics, Hokkaido University, Sapporo 060-0810, Japan

(Dated: November 30, 2018)

The previous investigation on Rayleigh-Bénard convection of a dilute classical gas [T. Kita: J. Phys. Soc. Jpn. **75** (2006) 124005] is extended to calculate entropy change of the convective transition with the rigid boundaries. We obtain results qualitatively similar to those of the stress-free boundaries. Above the critical Rayleigh number, the roll convection is realized among possible steady states with periodic structures, carrying the highest entropy as a function of macroscopic mechanical variables.

PACS numbers:

## I. INTRODUCTION

In a preceding paper,<sup>1</sup> we performed a statistical mechanical investigation on Rayleigh-Bénard convection of a dilute classical gas based on the Boltzmann equation. We specifically calculated entropy change through the convective transition for the case of the stress-free boundaries as a function of macroscopic mechanical variables. We thereby tested the validity of the principle of maximum entropy proposed for nonequilibrium steady states.<sup>2</sup> The present paper extends the consideration to a more realistic case of the rigid boundaries.<sup>3</sup>

## II. FORMULATION AND NUMERICAL PROCEDURES

Our starting point is Eq. (46) of ref. 1:

$$\frac{\partial T^{(1)}}{\partial t} + \hat{\mathbf{j}}^{(1.5)} \cdot \nabla T^{(1)} - \kappa^{(2)} \nabla^2 T^{(1)} = 0, \quad (1a)$$

$$\begin{aligned} -\frac{\partial}{\partial t} \nabla^2 \hat{\mathbf{j}}^{(1.5)} + \nabla \times \nabla \times (\hat{\mathbf{j}}^{(1.5)} \cdot \nabla \hat{\mathbf{j}}^{(1.5)}) \\ + \nu^{(2)} (\nabla^2)^2 \hat{\mathbf{j}}^{(1.5)} + U_g^{(2)} (\mathbf{e}_z \nabla^2 - \mathbf{e}_z \cdot \nabla \nabla) T^{(1)} = \mathbf{0}, \end{aligned} \quad (1b)$$

where  $\nabla \cdot \hat{\mathbf{j}}^{(1.5)} = \mathbf{0}$  and the units are described in §3.1. We adopt the condition of the rigid boundaries along  $z$ , i.e.,  $\hat{\mathbf{j}}^{(1.5)} = \mathbf{0}$  at  $z = \pm 1/2$ . Combined with  $\nabla \cdot \hat{\mathbf{j}}^{(1.5)} = \mathbf{0}$ , it yields the boundary conditions:

$$\hat{\mathbf{j}}_{\perp}^{(1.5)} \Big|_{z=\pm 1/2} = \mathbf{0}, \quad (2a)$$

$$\hat{j}_z^{(1.5)} \Big|_{z=\pm 1/2} = \frac{\partial \hat{j}_z^{(1.5)}}{\partial z} \Big|_{z=\pm 1/2} = 0, \quad (2b)$$

with  $\hat{\mathbf{j}}_{\perp}^{(1.5)}$  denoting the  $xy$  components. As for the horizontal directions, we consider the region  $-L/2 \leq x, y \leq L/2$  with  $L \gg 1$  and impose the periodic boundary conditions. We also fix macroscopic mechanical variables of

the system, i.e., the total particle number, energy, and energy flux along  $z$ . These conditions lead to eq. (42) of ref. 1, i.e.,

$$\int T^{(1)} d^3r = 0, \quad (3a)$$

$$\frac{1}{L^2} \int_{-L/2}^{L/2} dx \int_{-L/2}^{L/2} dy \frac{\partial T^{(1)}}{\partial z} \Big|_{z=-1/2} = -\Delta T_{\text{hc}}, \quad (3b)$$

where  $\Delta T_{\text{hc}} \equiv 2\bar{j}_Q^{(3)}/3\bar{n}\kappa^{(2)}$  denotes the temperature difference between  $z = \pm 1/2$  that would be realized in the heat-conducting state.

We solve the above equations with the method developed by Pesch.<sup>4</sup> First, the boundary conditions of eq. (2) is treated with the Galerkin method,<sup>5</sup> i.e., by expanding every  $z$  dependence in terms of some basis functions satisfying the boundary conditions. Specifically, the basis functions for eq. (2a) are obtained from the second-order differential equation  $S'' = -\lambda S$  with  $S(\pm 1/2) = 0$  as

$$S_n(z) = \sqrt{2} \sin n\pi(z+1/2) \quad (n = 1, 2, \dots). \quad (4a)$$

They satisfy  $\langle S_n | S_{n'} \rangle \equiv \int_{-1/2}^{1/2} S_n(z) S_{n'}(z) dz = \delta_{nn'}$ . On the other hand, those for eq. (2b) are constructed from the fourth-order differential equation  $C^{(4)} = k^4 C$  with  $C(\pm 1/2) = C'(\pm 1/2) = 0$  as

$$C_n(z) = \begin{cases} A_n \left( \frac{\cosh k_n z}{\cosh \frac{k_n}{2}} - \frac{\cos k_n z}{\cos \frac{k_n}{2}} \right) & : n = 1, 3, \dots \\ A_n \left( \frac{\sinh k_n z}{\sinh \frac{k_n}{2}} - \frac{\sin k_n z}{\sin \frac{k_n}{2}} \right) & : n = 2, 4, \dots \end{cases}, \quad (4b)$$

where  $k_n (> 0)$  is determined by

$$\begin{cases} \tanh \frac{k_n}{2} + \tan \frac{k_n}{2} = 0 & : n = 1, 3, \dots \\ \coth \frac{k_n}{2} - \cot \frac{k_n}{2} = 0 & : n = 2, 4, \dots \end{cases}. \quad (4c)$$

Note  $k_n \approx (n+1/2)\pi$  for  $n \gg 1$ . The quantity  $A_n$  is the normalization constant:

$$A_n = \begin{cases} \frac{\sqrt{2} \cosh \frac{k_n}{2} \cos \frac{k_n}{2}}{\sqrt{\cosh^2 \frac{k_n}{2} + \cos^2 \frac{k_n}{2}}} & : n = 1, 3, \dots \\ \frac{\sqrt{2} \sinh \frac{k_n}{2} \sin \frac{k_n}{2}}{\sqrt{\sinh^2 \frac{k_n}{2} - \sin^2 \frac{k_n}{2}}} & : n = 2, 4, \dots \end{cases}, \quad (4d)$$

so that  $\langle C_n | C_{n'} \rangle = \delta_{nn'}$ . The functions  $\{C_n(z)\}$  may be called Chandrasekhar functions.<sup>3</sup>

Now that appropriate basis functions are obtained, we expand  $T^{(1)}$  and  $\hat{\mathbf{j}}^{(1.5)}$  in eq. (1) as

$$T^{(1)}(\mathbf{r}) = -\Delta T z - T_1 + \sum_{\mathbf{k}_\perp} \sum_{n=1}^{\infty} \tilde{T}(\mathbf{k}_\perp, n) e^{i\mathbf{k}_\perp \cdot \mathbf{r}} S_n(z), \quad (5a)$$

$$\hat{j}_z^{(1.5)}(\mathbf{r}) = \sum_{\mathbf{k}_\perp \neq \mathbf{0}} \sum_{n=1}^{\infty} \tilde{j}_z(\mathbf{k}_\perp, n) e^{i\mathbf{k}_\perp \cdot \mathbf{r}} C_n(z), \quad (5b)$$

$$\hat{\mathbf{j}}_\perp^{(1.5)}(\mathbf{r}) = \sum_{\mathbf{k}_\perp \neq \mathbf{0}} \sum_{n=1}^{\infty} \tilde{\mathbf{j}}_\perp(\mathbf{k}_\perp, n) e^{i\mathbf{k}_\perp \cdot \mathbf{r}} S_n(z). \quad (5c)$$

Here  $\mathbf{k}_\perp = \mathbf{0}$  component is excluded in the expansion of  $\hat{\mathbf{j}}^{(1.5)}$  to seek only periodic current distributions in the  $xy$  plane. We have also incorporated into eq. (5a) the fact that the temperature is uniform at  $z = \pm 1/2$ . Now,  $\nabla \cdot \hat{\mathbf{j}}^{(1.5)} = \mathbf{0}$  is transformed into  $i\mathbf{k}_\perp \cdot \tilde{\mathbf{j}}_\perp(\mathbf{k}_\perp, n) + \sum_{n'} \langle S_n | C_{n'}' \rangle \tilde{j}_z(\mathbf{k}_\perp, n') = 0$ . It hence follows that  $\tilde{\mathbf{j}}_\perp(\mathbf{k}_\perp, n)$  can be expressed generally as

$$\begin{aligned} & \tilde{\mathbf{j}}_\perp(\mathbf{k}_\perp, n) \\ &= i \frac{\mathbf{k}_\perp}{k_\perp^2} \sum_{n'} \langle S_n | C_{n'}' \rangle \tilde{j}_z(\mathbf{k}_\perp, n') + \frac{\mathbf{e}_z \times \mathbf{k}_\perp}{k_\perp} \tilde{j}_p(\mathbf{k}_\perp, n). \end{aligned} \quad (6)$$

On the other hand, eq. (3) is transformed into

$$T_1 = \sum_{m=1}^{\infty} \frac{2\sqrt{2} \tilde{T}(\mathbf{0}, 2m-1)}{(2m-1)\pi}, \quad (7a)$$

$$\Delta T = \Delta T_{\text{hc}} + \sum_{n=1}^{\infty} \sqrt{2} n \pi \tilde{T}(\mathbf{0}, n). \quad (7b)$$

Let us substitute eq. (5) with eq. (6) into eq. (1) and perform space integrations using the orthonormality of the basis functions. We thereby obtain algebraic equations for the expansion coefficients as

$$\begin{aligned} & \frac{\partial \tilde{T}(\mathbf{k}_\perp, n)}{\partial t} + \kappa^{(2)} [k_\perp^2 + (n\pi)^2] \tilde{T}(\mathbf{k}_\perp, n) \\ & - \Delta T \sum_{n'} \langle S_n | C_{n'}' \rangle \tilde{j}_z(\mathbf{k}_\perp, n') \\ &= -\frac{1}{L^2} \langle e^{i\mathbf{k}_\perp \cdot \mathbf{r}} S_n | \hat{\mathbf{j}}^{(1.5)} \cdot \nabla \tilde{T}^{(1)} \rangle, \end{aligned} \quad (8a)$$

$$\begin{aligned} & \sum_{n'} (k_\perp^2 \delta_{nn'} - \langle C_n | C_{n'}'' \rangle) \frac{\partial \tilde{j}_z(\mathbf{k}_\perp, n')}{\partial t} \\ & + \nu^{(2)} \sum_{n'} [(k_\perp^4 + k_n^4)^2 \delta_{nn'} - 2k_\perp^2 \langle C_n | C_{n'}'' \rangle] \tilde{j}_z(\mathbf{k}_\perp, n') \\ & - U_g^{(2)} k_\perp^2 \sum_{n'} \langle C_n | S_{n'} \rangle \tilde{T}(\mathbf{k}_\perp, n') \\ &= -\frac{1}{L^2} \mathbf{e}_z \cdot \langle e^{i\mathbf{k}_\perp \cdot \mathbf{r}} C_n | \nabla \times \nabla \times (\hat{\mathbf{j}}^{(1.5)} \cdot \nabla \hat{\mathbf{j}}^{(1.5)}) \rangle, \end{aligned} \quad (8b)$$

$$\begin{aligned} & [k_\perp^2 + (n\pi)^2] \frac{\partial \tilde{j}_p(\mathbf{k}_\perp, n)}{\partial t} + \nu^{(2)} [k_\perp^2 + (n\pi)^2]^2 \tilde{j}_p(\mathbf{k}_\perp, n) \\ &= -\frac{1}{L^2} \frac{\mathbf{e}_z \times \mathbf{k}_\perp}{k_\perp} \cdot \langle e^{i\mathbf{k}_\perp \cdot \mathbf{r}} S_n | \nabla \times \nabla \times (\hat{\mathbf{j}}^{(1.5)} \cdot \nabla \hat{\mathbf{j}}^{(1.5)}) \rangle, \end{aligned} \quad (8c)$$

with  $\langle f | g \rangle \equiv \int_{-L/2}^{L/2} dx \int_{-L/2}^{L/2} dy \int_{-1/2}^{1/2} dz f^*(\mathbf{r}) g(\mathbf{r})$ .

Finally, entropy characteristic of convection is obtained by substituting eq. (5a) into eq. (50) of ref. 1 as

$$\begin{aligned} S^{(2)} &= -\frac{5}{4} \left\{ -T_1^2 + \frac{(\Delta T)^2}{12} + \sum_{\mathbf{k}_\perp} \sum_{n=1}^{\infty} |\tilde{T}(\mathbf{k}_\perp, n)|^2 \right. \\ & \quad \left. + \Delta T \sum_{m=1}^{\infty} \frac{\sqrt{2} \tilde{T}(\mathbf{0}, 2m)}{m\pi} \right\}, \end{aligned} \quad (9)$$

with  $T_1$  and  $\Delta T$  given by eq. (7).

It follows from the stability analysis for the heat-conducting state<sup>3</sup> that the critical Rayleigh number  $R_c$  is determined from eq. (8) by setting the nonlinear terms and time derivatives equal to zero. The relevant instability originates from the linear coupled equations for  $\tilde{T}(\mathbf{k}, n)$  and  $\tilde{j}_z(\mathbf{k}, n)$ . Eliminating  $\tilde{T}(\mathbf{k}, n)$  in favor of  $\tilde{j}_z(\mathbf{k}, n)$ , we obtain the equation for  $R_c$  as

$$\det \underline{A} = 0, \quad (10)$$

where matrix  $\underline{A}$  is defined by

$$\begin{aligned} A_{nn'} &\equiv (k_\perp^4 + k_n^4)^2 \delta_{nn'} - 2k_\perp^2 \langle C_n | C_{n'}'' \rangle \\ & \quad - R^{(-1)} k_\perp^2 \sum_{n''} \frac{\langle C_n | S_{n''} \rangle \langle S_{n''} | C_{n'} \rangle}{k_\perp^2 + (n''\pi)^2}, \end{aligned} \quad (11)$$

with

$$R^{(-1)} \equiv \frac{U_g^{(2)} \Delta T}{\nu^{(2)} \kappa^{(2)}}. \quad (12)$$

The critical Rayleigh number  $R_c$  corresponds to the minimum value of  $R^{(-1)}$  in eq. (10) as a function of  $k_\perp$ . Equation (10) is solved by approximating  $\underline{A}$  by a finite dimension of  $n_c \times n_c$ , and the convergence is checked by increasing  $n_c$ . Choosing  $n_c = 4$  already yields an excellent result of  $R_c = 1.708$  with  $k_\perp = 3.116 \equiv k_c$ .<sup>3</sup>

The nonlinear terms become relevant in eq. (8) for  $R^{(-1)} > R_c$ . They are evaluated for given expansion coefficients  $\tilde{T}(\mathbf{k}_\perp, n)$  and  $\tilde{\mathbf{j}}(\mathbf{k}_\perp, n)$  as follows. We first

construct  $T^{(1)}(\mathbf{r})$  and  $\hat{\mathbf{j}}^{(1.5)}(\mathbf{r})$  by eqs. (5)-(7). The fast Fourier transform (FFT)<sup>6</sup> is used in this procedure to obtain the  $xy$  dependence. We then perform the space differentiations numerically in the  $xy$  plane and analytically along the  $z$  direction. We specifically use the following formulas of  $O(h^6)$  in the  $xy$  plane:

$$\partial_x f(x, y) \approx \sum_{\sigma=\pm} \frac{\sigma}{60h} [f(x+3\sigma h, y) - 9f(x+2\sigma h, y) + 45f(x+\sigma h, y)], \quad (13a)$$

$$\partial_x^2 f(x, y) \approx \frac{1}{180h^2} \left\{ \sum_{\sigma=\pm} [2f(x+3\sigma h, y) - 27f(x+2\sigma h, y) + 270f(x+\sigma h, y)] - 490f(x, y) \right\}. \quad (13b)$$

The quantity  $\partial_{xy} f(x, y)$  is obtained with eq. (13a) by averaging the derivatives performed in different order. The nonlinear overlap integrals are evaluated finally, where we again use the FFT in the  $xy$  plane. On the other hand, all the calculations along  $z$  are performed by preparing the relevant overlap integrals in advance, e.g.,  $\langle S_n | S_{n'} S_{n''} \rangle$  and  $\langle S_n | C_{n'} S_{n''} \rangle$  for eq. (8a), and performing the summations over  $n'$  and  $n''$ .

Time evolutions of eq. (8) are calculated as follows. We first multiply eqs. (8b) and (8c) by  $(\underline{\mathcal{Q}}^{-1})_{n'n}$  and  $[k_\perp^2 + (n\pi)^2]^{-1}$  with  $(\underline{\mathcal{Q}})_{nn'} \equiv k_\perp^2 \delta_{nn'} - \langle C_n | C_{n'} \rangle$ , respectively, and perform summation over  $n$  for eq. (8b). Time integrations are then carried out numerically by treating  $\partial \mathbf{f} / \partial t = \mathbf{g}$  as  $\mathbf{f}(t + \Delta t) \approx \mathbf{f}(t) + \mathbf{g}(t) \Delta t$ . A disadvantage of this simple method is that we have to make  $\Delta t$  small enough to avoid an explosion in the numerical time integration. One may alternatively use the split-step integration scheme developed by Pesch which approximates  $\partial \mathbf{f} / \partial t = \underline{\mathbf{L}} \mathbf{f} + \mathbf{g}$  as  $\mathbf{f}(t + \Delta t) \approx e^{\underline{\mathbf{L}} \Delta t} \mathbf{f}(t) + e^{\underline{\mathbf{L}} \Delta t / 2} [3\mathbf{g}(t) - \mathbf{g}(t - \Delta t)] \Delta t / 2$ , thereby treating the linear part  $\underline{\mathbf{L}} \mathbf{f}$  exactly. This latter scheme removes the explosion at the expense of larger numerical errors to make a rapid time integration possible; the extra computational time for diagonalizing  $\underline{\mathbf{L}}$  in the calculation of  $e^{\underline{\mathbf{L}} \Delta t}$  is negligible in the whole numerical procedures.

We here focus on periodic solutions of eq. (1) in the  $xy$  plane and express  $\mathbf{r}_\perp = s_1 \mathbf{a}_1 + s_2 \mathbf{a}_2$ , where  $\mathbf{a}_1 \equiv (a_{1x}, a_{1y}, 0)$  and  $\mathbf{a}_2 \equiv (0, a_2, 0)$  denote the basic vectors. Accordingly, we adopt the periodic boundary condition for the region spanned by  $\mathcal{N}_1 \mathbf{a}_1$  and  $\mathcal{N}_2 \mathbf{a}_2$  with  $\mathcal{N}_j$  ( $j = 1, 2$ ) a large integer. The above theoretical framework can also be used in this case with a minor modification. Indeed, we only have to perform the change of variables  $(x, y) \rightarrow (s_1, s_2)$  in the  $xy$  integrations of the nonlinear terms. Those integrations have to be carried out now only over the unit cell of  $0 \leq s_1, s_2 \leq 1$ . The corresponding wave vector  $\mathbf{k}_\perp$  is given by  $\mathbf{k}_\perp = \ell_1 \mathbf{b}_1 + \ell_2 \mathbf{b}_2$ , where  $\mathbf{b}_1 \equiv 2\pi(\mathbf{a}_2 \times \mathbf{e}_z) / [(\mathbf{a}_1 \times \mathbf{a}_2) \cdot \mathbf{e}_z]$ ,  $\mathbf{b}_2 \equiv 2\pi(\mathbf{e}_z \times \mathbf{a}_1) / [(\mathbf{a}_1 \times \mathbf{a}_2) \cdot \mathbf{e}_z]$ , and  $\ell_j$  denotes an integer. The linear stability analysis for the heat-conducting state suggests that the stable solution satisfies  $|\mathbf{b}_1| \sim |\mathbf{b}_2| \sim k_c = 3.116$ .

The parameters in eq. (8) are chosen the same as those used for the free boundaries, i.e., eq. (37a) of ref. 1, which correspond to Ar at 273K under atmospheric pressure. We also fix the heat-flux density  $\bar{j}_Q^{(3)}$  at  $z = -1/2$  so that the temperature difference  $\Delta T_{\text{hc}} = 1\text{K}$  is realized between  $z = \pm 1/2$  in the heat-conducting state. The Rayleigh number  $R^{(-1)}$  is controlled by changing the thickness  $d$ .

Practical calculations of eq. (8) are performed as follows: We first multiply eqs. (8a)-(8c) by  $10^8$ ,  $10^{10}$  and  $10^{10}$ , respectively, and rewrite them in terms of  $\tilde{T}'(\mathbf{k}_\perp, n) \equiv 10^3 \tilde{T}(\mathbf{k}_\perp, n)$  and  $\tilde{j}'(\mathbf{k}_\perp, n) \equiv 10^5 \tilde{j}(\mathbf{k}_\perp, n)$  to obtain equations of  $O(1)$ . The summations over  $n$  are truncated at a finite value  $n_c$ , whereas  $N_{\text{FFT}}$  discrete points are used to perform FFT for each direction in the  $xy$  plane. As for periodic structures, we investigate the three candidates: the roll, the square lattice and the hexagonal lattice with  $|\mathbf{b}_1| = |\mathbf{b}_2| \sim k_c$ . We then trace time evolutions of the expansion coefficients until they all acquire constant values. Choosing  $\Delta t \lesssim 0.005$ ,  $n_c \gtrsim 4$  and  $N_{\text{FFT}} \gtrsim 2^4$  yields excellent convergence for the calculations presented below even with the simplest time-integration scheme. The initial state is chosen as the conducting state with small fluctuations  $\tilde{T}'(\mathbf{k}_\perp, 1) \sim 10^{-2}$  for the basic harmonics  $\mathbf{k}_\perp$ . The constants  $\Delta T$  and  $T_1$  are updated at each time step by using eq. (7). Also evaluated at each time step is entropy measured with respect to the heat-conducting state:

$$\Delta S \equiv S^{(2)} - S_{\text{hc}}^{(2)}, \quad (14)$$

where  $S^{(2)}$  is given by eq. (9) and  $S_{\text{hc}}^{(2)} = -5(\Delta T_{\text{hc}})^2 / 48$ . We thereby trace time evolution of  $\Delta S$  simultaneously. The above procedure is carried out for each fixed periodic structure.

One of the advantages of the present approach is that we only have to change the basis functions to study other boundary conditions. For example, the case of the stress-free boundaries can also be treated within the present framework by simply changing  $C_n(z) \rightarrow S_n(z)$  and  $S_n(z) \rightarrow \sqrt{2} \cos n\pi(z + 1/2)$  in the expansions of eqs. (5b) and (5c), respectively. This replacement has been checked to reproduce the results obtained in ref. 1 appropriately.

### III. RESULTS

We now present numerical results on the rigid boundaries, which turn out to be qualitatively the same as those of the stress-free boundaries.<sup>1</sup>

Figure 1 shows time evolution of  $\Delta S$  for the Rayleigh number  $R^{(-1)} = 1.2R_c$ . The letters r, s and h denote (r) roll, (s) square and (h) hexagonal, respectively, distinguishing initial conditions; they are exactly the same as those for the stress-free boundaries.<sup>1</sup> Writing  $\tilde{T}'(\mathbf{k}_\perp, n) = \tilde{T}'[\ell_1, \ell_2, n]$  and introducing the angle  $\theta$  by  $\theta \equiv \cos^{-1}(\mathbf{b}_1 \cdot \mathbf{b}_2)$ , those initial conditions are given explicitly as follows: (r)  $\tilde{T}'[\pm 1, 0, 1] = 1.00 \times 10^{-2} / \sqrt{8}$

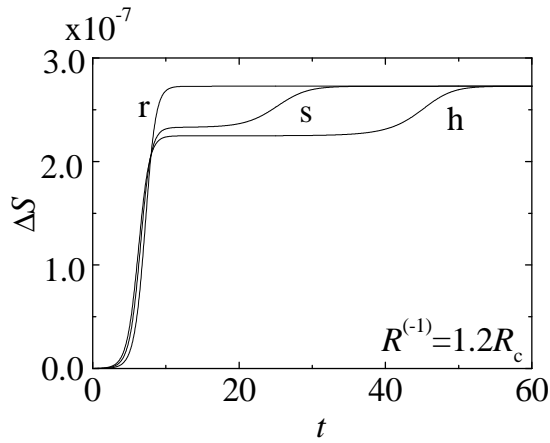


FIG. 1: Time evolution of entropy measured with respect to the heat-conducting state for  $R^{(-1)} = 1.2R_c$ . The letters r, s and h denote roll, square and hexagonal, respectively, distinguishing initial fluctuations around the heat-conducting solution; see text for details. The final state of  $t \gtrsim 50$  is the roll convection, whereas the intermediate plateaus of s and h correspond to the square and hexagonal convections, respectively.

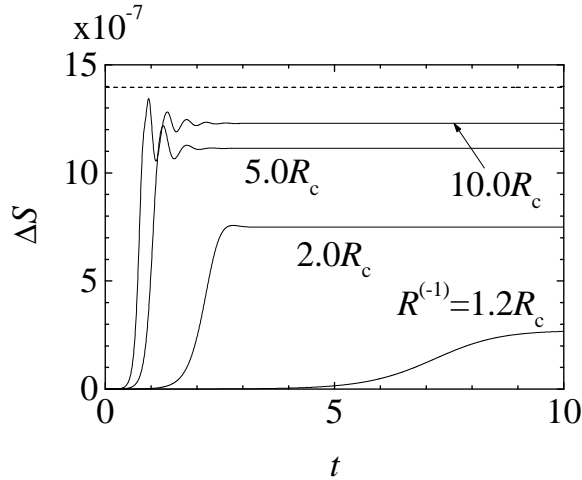


FIG. 2: Time evolution of entropy  $\Delta S$ . The four curves correspond to the different Rayleigh numbers:  $R^{(-1)} = 1.2R_c$ ,  $2.0R_c$ ,  $5.0R_c$  and  $10.0R_c$ . The initial state is the heat-conducting state with the fluctuation  $\tilde{T}'[\pm 1, 0, 1] = 1.0 \times 10^{-2}/\sqrt{8}$  and  $|\mathbf{b}_1| = k_c$ , whereas all the final states are the roll convection. The broken line near the top indicates the upper bound of  $\Delta S$ .

with  $|\mathbf{b}_1| = k_c$ ; (s)  $\tilde{T}'[\pm 1, 0, 1] = 1.01 \times 10^{-2}/\sqrt{8}$  and  $\tilde{T}'[0, \pm 1, 1] = 0.99 \times 10^{-2}/\sqrt{8}$  with  $|\mathbf{b}_1| = |\mathbf{b}_2| = k_c$  and  $\theta = \pi/2$ ; (h)  $\tilde{T}'[\pm 1, 0, 1] = \tilde{T}'[0, \pm 1, 1] = 1.00 \times 10^{-2}/\sqrt{8}$  and  $\tilde{T}'[1, 1, 1] = \tilde{T}'[-1, -1, 1] = 1.01 \times 10^{-2}/\sqrt{8}$  with  $|\mathbf{b}_1| = |\mathbf{b}_2| = k_c$  and  $\theta = 2\pi/3$ . We observe clearly that entropy increases monotonically in all the three

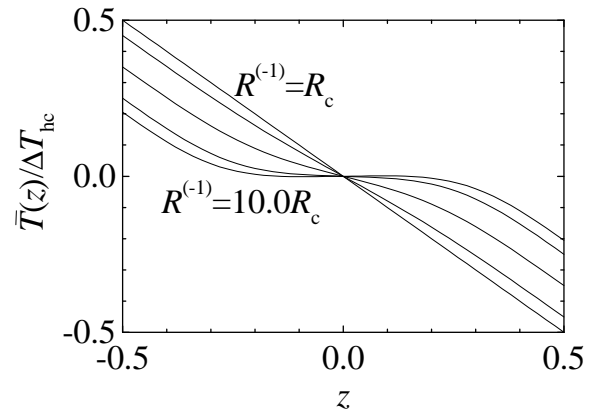


FIG. 3: Profile of the average temperature variation  $\bar{T}(z)$  in the roll convection normalized by the temperature difference  $\Delta T_{hc}$  in the heat-conducting state. The Rayleigh numbers are  $R^{(-1)} = R_c, 1.2R_c, 2.0R_c, 5.0R_c$  and  $10.0R_c$  from top to bottom on the left part.

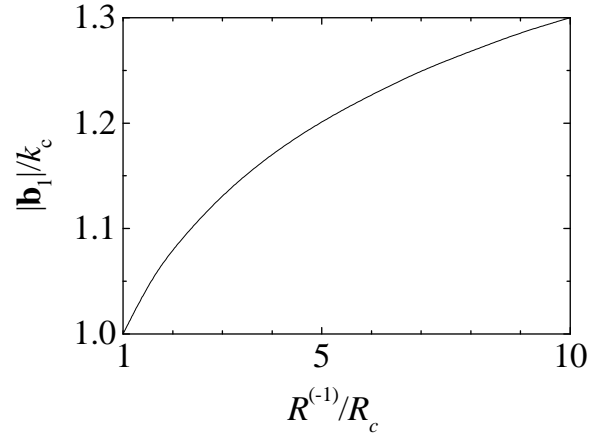


FIG. 4: The length  $|\mathbf{b}_1|/k_c$  of the stable roll convection as a function of the normalized Rayleigh number  $R^{(-1)}/R_c$ .

cases to reach a common final value of the roll convection. The intermediate plateaus seen in s and h correspond to the metastable square and hexagonal lattices, respectively, with (s)  $\tilde{T}'[\pm 1, 0, 1] \sim \tilde{T}'[0, \pm 1, 1]$  and (h)  $\tilde{T}'[\pm 1, 0, 1] \sim \tilde{T}'[0, \pm 1, 1] \sim \tilde{T}'[\pm 1, \pm 1, 1]$ .

Figure 2 displays time evolution of  $\Delta S$  for four different Rayleigh numbers, all developing from the initial fluctuation  $\tilde{T}'[\pm 1, 0, 1] = 1.00 \times 10^{-2}/\sqrt{8}$  with  $|\mathbf{b}_1| = k_c$ . Each final state is the roll convection. Compared with the case of the stress-free boundaries,<sup>1</sup> we observe an enhanced oscillatory behavior for  $R = 5.0R_c$  and  $10.0R_c$  after the first rapid increase of  $\Delta S$ .

Figure 3 shows profile of the average temperature variation  $\bar{T}(z)$  along  $z$  in the roll convection for five different Rayleigh numbers. Figure 4 plots  $|\mathbf{b}_1|/k_c$  corresponding to the maximum of  $\Delta S$  as a function of  $R^{(-1)}/R_c$ . Again

the basic features are qualitatively the same as those of the stress-free boundaries.<sup>1</sup>

Thus, we have seen that the principle of maximum entropy proposed in ref. 2 is satisfied through the Rayleigh-Bénard convective transition of a dilute classical gas even in the realistic case of the rigid boundaries.

### Acknowledgments

I would like to thank W. Pesch for explaining his method to solve the Boussinesq equations. This work

is supported in part by the 21st century COE program “Topological Science and Technology,” Hokkaido University.

---

<sup>1</sup> T. Kita: J. Phys. Soc. Jpn. **75** (2006) 124005; **76** (2007) 038001.

<sup>2</sup> T. Kita: J. Phys. Soc. Jpn. **75** (2006) 114005.

<sup>3</sup> S. Chandrasekhar: *Hydrodynamic and Hydromagnetic Stability* (Clarendon Press, Oxford, 1961).

<sup>4</sup> W. Pesch: Chaos **6** (1996) 348.

<sup>5</sup> See, e.g., D. Gottlieb and S. A. Orszag: *Numerical Analysis*

*of Spectral Methods: Theory and Applications* (Society for Industrial and Applied Mathematics, Philadelphia, 1977),

<sup>6</sup> See, e.g., W. H. Press, S. A. Teukolsky, W. T. Vetterling and B. P. Flannery: *Numerical Recipes in C* (Cambridge University Press, Cambridge, 1992).